SCIENCE CHINA
Earth Sciences

•ARTICLE•

September 2025 Vol.68 No.9: 3024–3034
https://doi.org/10.1007/s11430-025-1646-9

Clay mineral controlling REY enrichment in marine phosphorites

Shengwei WU[1,2], Haifeng FAN[2*], Fasheng LOU[1], Shan HE[3], Yong XIA[2], Xiqiang LIU[2], Haiying YANG[4], Xingxiang GONG[5] & Hanjie WEN[6]

[1] *Jiangxi Province Key Laboratory of Exploration and Development of Critical Mineral Resources, Jiangxi Geological Survey and Exploration Institute, Nanchang 330009, China*
[2] *State Key Laboratory of Critical Mineral Research and Exploration, Institute of Geochemistry, Chinese Academy of Sciences, Guiyang 550081, China*
[3] *Langfang Natural Resources Comprehensive Survey Center, China Geological Survey, Langfang 065000, China*
[4] *School of Earth Sciences, Yunnan University, Kunming 650500, China*
[5] *Reserve Bureau of Land and Mineral Resources of Guizhou Province, Guiyang 550081, China*
[6] *School of Earth Sciences and Resources, Chang'an University, Xi'an 710054, China*

Received March 7, 2025; revised June 24, 2025; accepted July 15, 2025; published online August 12, 2025

Abstract With the global vigorous development of high-tech industries, the market demand for rare earth elements and Yttrium (REY) have experienced explosive growth. In recent years, phosphate associated REY resources (up to 18,000 ppm) found in modern deep-sea muds have attracted significant attentions. It is believed that their REY originated directly from porewater in deep-sea sediments, with a process of detrital dissolution releasing REY into the porewater. However, it remains unclear whether this model could be applied to REY-rich phosphorites from geological history, which contrasts sharply with the widely accepted Fe-oxide redox pump model at the seawater-sediment interface. Here, we present the mineralogy and REY geochemistry of clay minerals, and whole-rock Si-Fe isotopic compositions (δ^{30}Si and δ^{56}Fe) from early Cambrian REY-rich Zhijin phosphorite ($\sum$REY, ~2000 ppm) and REY-poor Meishucun phosphorite ($\sum$REY, <400 ppm) in South China. In the Zhijin samples, illite formed around the edges of muscovite, exhibiting seawater-like REY patterns. In contrast, muscovite and orthoclase in the Meishucun samples show no contact relationship and display REY patterns typical of granite-forming minerals. The REY contents (reach 310 ppm) of muscovites from Zhijin samples are much higher than that of detrital muscovite (REY, 0.09–5.86 ppm) and orthoclase (REY, 2.69–6.45 ppm) from Meishucun samples. Furthermore, the data can be classified into two categories based on the correlation between δ^{30}Si values and phosphate-hosted REY enrichment in Zhijin and Meishucun samples. One is characterized by higher δ^{30}Si values (average 0.6‰) and Y/Ho ratios (average 56), and lower SiO_2 and REY contents (average 8.10% and 1076 ppm, respectively). The other group exhibits lower δ^{30}Si values (average 0.2‰) and Y/Ho ratios (average 52), and higher SiO_2 and REY contents (average 17.45% and 2085 ppm, respectively). In addition, compared to the Meishucun phosphorites formed in well oxidized marine environment (δ^{56}Fe, ~0‰), the Zhijin phosphorites developed under fluctuating oxic-suboxic marine condition exhibit a significant negative correlation between Fe and Si isotopic compositions. These findings indicate Zhijin muscovite underwent REY exchange with seawater under fluctuating redox marine conditions, leading to REY release into the porewater and the formation of authigenic illite. This process did not occur in the Meishucun samples. It's well known that continental weathering transformed feldspar into REY-rich muscovite or illite. These REY-rich clays, transported to the seawater-sediment interface, were dissolved and released REY into the porewater within a fluctuating oxic-suboxic marine environment. We proposed for the first time that fluctuating marine redox conditions acted as a trigger for REY enrichment in ancient phosphorites, with the primary REY source being terrigenous REY-rich clay. This perspective not only provides an insight into the mechanism of REY enrichment in phosphorites, but could also account for the lack of anomalous REY enrichment in phosphorites exhibiting the precipitation of extensive pyrites if only Fe-oxide redox processes are considered.

* Corresponding author (email: fanhaifeng@mail.gyig.ac.cn)

Keywords Marine phosphorite, REY enrichment, Clay mineral, Silicate alteration, Redox conditions

Citation: Wu S, Fan H, Lou F, He S, Xia Y, Liu X, Yang H, Gong X, Wen H. 2025. Clay mineral controlling REY enrichment in marine phosphorites. Science China Earth Sciences, 68(9): 3024–3034, https://doi.org/10.1007/s11430-025-1646-9

1. Introduction

Modern marine phosphates are known for their abundant rare earth elements and Yttrium (REY) concentrations, which primarily originated from porewater, with Fe-oxides facilitating REY release through anoxic reduction (Haley et al., 2004). However, clay minerals such as smectite, illite, and kaolinite in oceanic sediments, also significantly contribute to porewater REY enrichment for several seasons: (1) Higher REY content in Red clay: Red clays from the North Atlantic (257 ppm, 1 ppm=1 mg/L) and Eastern South Pacific (1180 ppm) (Menendez et al., 2017), have much higher REY content than Fe-oxides (2.76–15.6 ppm) (Paul et al., 2019). (2) The Sr-Nd isotopic compositions ($^{87}Sr/^{86}Sr$, 0.7083–0.7092 and 0.7091–0.7121; ε_{Nd}, −6.41 to −5.14 and −7.38 to −5.82) in phosphate fractions and non-phosphate components (e.g., phillipsite and clay) indicated a strong terrigenous contribution from the Western Pacific sediments (Ren et al., 2022). The dissolution of these terrigenous particles (e.g., Sr, Nd release of 0.5%–10%) occurred over a relatively short timescale of weeks to months (Jeandel and Oelkers, 2015). (3) The REY signature of World River Average Clay mirrors the REY-rich porewater pattern (Abbott et al., 2019). Additionally, closed-system experiment demonstrated that seawater reacting with detrital materials lead to light REY enrichment (Adebayo et al., 2022). (4) The detrital dissolution model has been successfully applied to explain REY enrichment in Western Pacific sediments (Deng et al., 2022; Wang et al., 2024). Hence, the dissolution of continental particulate matter played a crucial role in delivering REY to modern seawater (Jeandel and Oelkers, 2015).

Similarly, phosphorites have consistently shown significant REY enrichment throughout geological history (Emsbo et al., 2015). Historically, the reduction of Fe-oxides has been considered the primary mechanism for REY enrichment, evidenced by mineralogic, element geochemical, and heavy Fe isotopic signatures (Zhang et al., 2022; Xing et al., 2024). However, this Fe-oxide reduction dissolution model is now being questioned. We observed that the presence of diagenetic pyrite does not always correlate with REY enrichment in phosphorites. For example, lower Cambrian phosphorites from northern Iran (∑REY=~200 ppm), challenge this model (Abedini and Calagari, 2017). However, in Permian-Triassic strata from South China, clay contents exhibit a strong positive correlation with REY contents of conodonts (Zhao et al., 2013). REY-rich phosphorites (∑REY, >1000 ppm) typically display distinct terrestrial REY signatures. For instance, Late Ediacaran-Cambrian phosphorites show terrigenous Y/Ho ratios (25–30) and were linked to felsic to mafic source rocks from the East European Platform and the Georgina Basin in Australia (Francovschi et al., 2020; Valetich et al., 2022). These studies suggested that the terrigenous supply of REY cannot be ignored, though it remains uncertain whether the dissolution of terrigenous clay significantly contributed to REY enrichment in historical phosphorites.

To better understand the mechanism behind REY enrichment in phosphorites, we investigated early Cambrian REY-rich Zhijin and REY-poor Meishucun phosphorites from the Yangtze Block, using mineralogy, elemental geochemistry, and Si-Fe isotopic compositions ($\delta^{30}Si$ and $\delta^{56}Fe$). This research not only provides new insight into the REY enrichment process in marine phosphorites, but also offers a fresh perspective on the REY geochemical cycle between the continents and marine sediments throughout geological time.

2. Geological setting

During the Early Cambrian, Yangtze plate mainly developed carbonate deposit (shelf), carbonate and black shale interbedding (slope), and black shale and chert deposit (basin), wherein shelf facies preserved thickly bedded phosphorites (Gao et al., 2018) (Figure 1). Zhijin phosphorite deposit with REY contents of ~2000 ppm, locates in Zhijin County, Guizhou province, was found in the Gezhongwu Formation (~20 m thickness), underlain by the Dengying Formation (dolostones) and overlain by the Niutitang Formation (black shales) (Zhang et al., 2022). Meishucun phosphorite deposit with REY contents of <400 ppm, approximately 10 m thickness, is situated in Jinning County, Yunnan province, within the Zhongyicun Member, underlain by the Xiaowaitoushan Member (dolostones) and overlain by the Dahai Member (dolostones) (Liu and Zhou, 2017). A volcanic tuff layer in the middle Zhongyicun Member has a zircon U-Pb age of 535.2±1.7 Ma (Zhu et al., 2009). The zircon U-Pb age of bentonites at the top of Dahai Member is 526.5±1.1 Ma (Compston et al., 2008), similar to the Re-Os age (521±5 Ma) of the Ni-Mo sulfide layer at the top of the Gezhongwu Formation (Xu et al., 2011).

3. Sampling and analytical methods

3.1 Samples

Samples were collected from the Zhijin and Meishucun

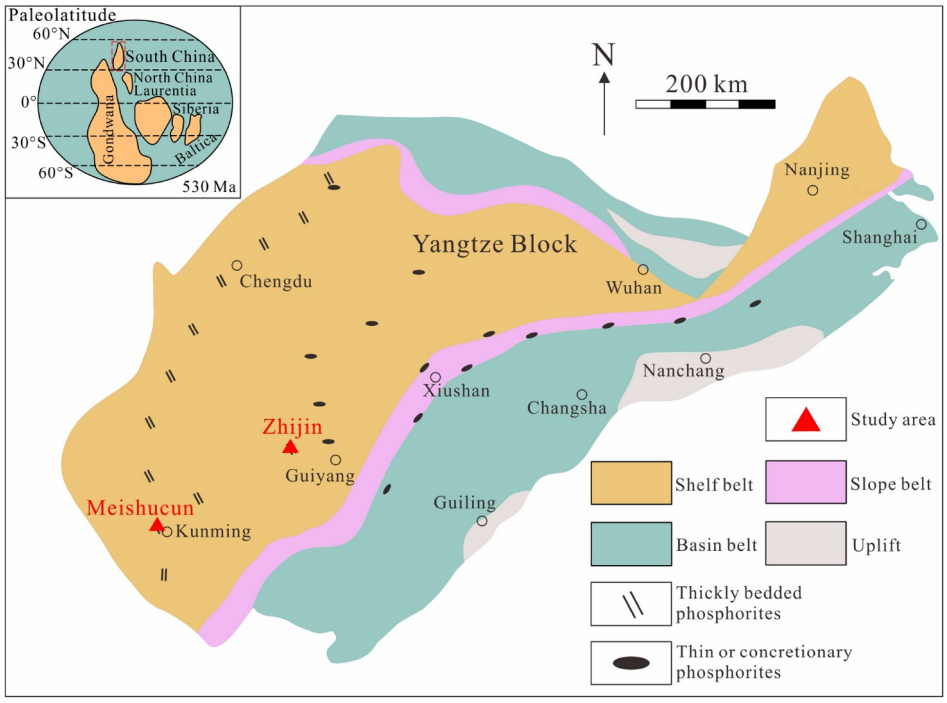

Figure 1 Early Cambrian sedimentary paleogeography from South China (modified from Gao et al. (2018) and Zhang et al. (2022)).

phosphorite deposits in Guizhou and Yunnan provinces, China, respectively, wherein the samples from Zhijin phosphorite deposit include Motianchong, Gaoshan, and Maoping ore blocks (Appendix Figures S1–S2). Vein material was removed to ensure sample uniformity, and the remaining samples were ground to a fine powder (200 mesh) for elemental and isotopic geochemical analysis. Some samples were also prepared as thin sections for mineralogical examination and *in-situ* REY analysis.

3.2 Methods

3.2.1 TESCAN Intergrated Mineral Analyzer (TIMA)

The analysis was conducted on thin sections using a MIRA3 scanning electron microscope. The parameters were set as follows: acceleration voltage of 25 kV, current of 8.24 nA, working distance of 15 mm, pixel spacing of 2 μm, and dot spacing of 6 μm. The current and BSE signal strength were calibrated on a platinum Faraday cup using an automatic program, while the EDS signal was calibrated with a Mn standard sample.

3.2.2 Whole-rock major elements and REY analysis

For major element analysis, samples in a platinum crucible were melted using a mixed flux ($Li_2B_4O_7$-$LiBO_2$-$LiNO_3$) at 1050°C and analyzed by X-ray fluorescence spectrometer. Standard materials (GBW07211, GBW07237, and GBW07241) ensured data reliability, with accuracy and precision controlled within 7.5%.

For REY analysis, samples were dissolved in nitric, hydrochloric, and hydrofluoric acids and analyzed by ICP-MS. Standard materials (OREAS-100a, OREAS-120, and STSD-1) ensured data reliability, with accuracy and precision within 10%.

3.2.3 In-situ REY analysis

REY concentrations in muscovite, illite, and orthoclase were analyzed using laser ablation inductively coupled plasma mass spectrometry (LA-ICP-MS). The analytical system consisted of a New Wave Research 193 nm ArF Excimer laser ablation unit coupled with a Thermo Scientific iCAP RQ quadrupole ICP-MS. Helium served as the carrier gas. The laser parameters employed in this study included a spot size of 30 μm, energy density of 3.5 J/cm^2 and frequence of 6 Hz, respectively. Glass NIST610, NIST612, and BHVO-2G were used as external standards for trace element calibration. Each analysis involved approximately 40 s of background acquisition, followed by 45 s of signal acquisition from the sample. Data processing was conducted using ICPMSDataCal software. Detailed analytical procedures have been described by Liu et al. (2008).

3.2.4 Whole-rock Si and Fe isotopic compositions analysis

Silicon isotopic compositions (δ^{30}Si) were conducted using the SiF_4 method described by Ding (2004). Following precise weighing, samples were digested with 6 mol/L HCl for ≥ 8 hours to eliminate carbonate and phosphate contaminants. After centrifugation, the residue underwent repeated rinsing

cycles with deionized water, followed by centrifugation, until a neutral pH was achieved. The sample was then transferred to a muffle furnace and ashed for 4 hours to remove organic matter, resulting in silicon enrichment. The silicon-enriched product was reacted with BrF_5 under vacuum conditions to quantitatively convert silicates into SiF_4 gas. The generated SiF_4 was purified and analyzed using a MAT-253 gas-source isotope ratio mass spectrometer. The δ^{30}Si was determined relative to NBS-28 (δ^{30}Si=0‰). Instrument stability was monitored using a standard reference material (GBW04421, δ^{30}Si=−0.02‰), ensuring a precision of better than ±0.1‰ for δ^{30}Si.

For Fe isotopic compositions (δ^{56}Fe) analysis, the pretreatment procedures for phosphorite samples and the instrumentation used for isotopic measurements (MC-ICP-MS) strictly followed the methodology detailed in Zhang et al. (2022). The δ^{56}Fe values of the samples were reported as relative to the reference material IRMM-524A. The standard sample (BCR-2, δ^{56}Fe=0.13‰±0.06‰) was used to monitor instrument stability during sample testing.

4. Results

4.1 Mineralogic characteristics

Zhijin quartz and pyrite grew within the illite matrix, with illite forming around muscovite edges and residual muscovite along pyrite margins (Figure 2a, 2b). In contrast, Meishucun orthoclase and muscovite were randomly distributed without clear contact between them (Figure 2c), wherein trace amounts of illites were occasionally observed along muscovite margin (Figures S3a, S3b).

4.2 Whole-rock compositions and *in-situ* REY from phosphorites

Zhijin muscovites and illites have REY contents ranging from 37.9 to 310 ppm and 0.44 to 3.49 ppm, respectively, while Meishucun orthoclases and muscovites have REY contents of 2.69–6.45 ppm and 0.09–5.86 ppm, respectively. PAAS-normalized REY patterns of Zhijin muscovites and illites align with those of modern seawater, Zhijin dolomites, and Fe-oxides, showing heavy REY enrichment (Figure 2d, 2e). In contrast, Meishucun orthoclases and muscovites have flat REY patterns similar to rock-forming minerals in granites (Figure 2f). Zhijin phosphorites show Al_2O_3 contents and Al/Si ratios of 0.18%–12.34% and 0.01–0.49, respectively. Meishucun phosphorites exhibit REY contents, Al_2O_3 contents, and Al/Si ratios of 87–462 ppm, 0.10%–3.90%, and 0.04–0.26, respectively. Overall, Zhijin samples generally have higher Al contents and Al/Si ratios, compared to Meishucun samples (Figure S4a and Appendix Tables).

4.3 Whole-rock δ^{30}Si and δ^{56}Fe of the Zhijin and Meishucun samples

The δ^{30}Si values of Zhijin samples range from −0.2‰ to 0.9‰ (average 0.4‰), while those of the Meishucun samples range from 0.2‰ to 0.9‰ (average 0.6‰). Zhijin samples fall between the seawater and clay endmembers, while Meishucun samples are closer to the seawater endmember (Figure S4a). Both sample sets can be divided into two groups: one with higher δ^{30}Si values (0.2‰ to 0.9‰, average 0.6‰) and Y/Ho ratios (48–68, average 56), lower REY (244–2066 ppm, average 1076 ppm) and SiO_2 contents (2.36%–25.61%, average 8.10%); and another with lower δ^{30}Si values (−0.2‰ to 0.5‰, average 0.2‰) and Y/Ho ratios (46–55, average 52), but higher REY (1499–2928 ppm, average 2085 ppm) and SiO_2 contents (8.23%–42.43%, average 17.45%) (Figure 3a–3c).

The δ^{56}Fe values of Zhijin phosphorites range from 0.08‰ to 0.52‰ (average 0.27‰), which exhibit a positive correlation with their REY contents (Figure S5a). Moreover, the δ^{56}Fe values of Zhijin phosphorites show a negative correlation with their δ^{30}Si values (Figure 3d).

5. Discussion

5.1 Genesis of clay minerals in Zhijin phosphorite

In the epigenetic weathering systems, potassium feldspar undergoes alteration to form muscovite and illite, with muscovite further transforming into illite (Berner and Holdren, 1977; Yuan et al., 2019). In marine environment, silicate alteration can also produce authigenic clay minerals through seawater-particle interactions (Geilert et al., 2023), resulting in element and isotope exchanges between seawater and silicate minerals. Therefore, it is essential to determine whether the clay minerals in the samples are of clastic or authigenic origin. Several key indicators can help distinguish between the two. Firstly, scanning electron microscope (SEM) or electron microprobe images (EPMA) reveal specific contact relationships between authigenic and clastic minerals. For instance, clastic quartz and feldspar grains have been observed embedded within authigenic clays (e.g., illite and smectite) in sediments from the Eastern North Pacific and the Peruvian margin (Abbott et al., 2019; Geilert et al., 2023). Secondly, distinct REY concentrations and patterns can be observed in clastic versus authigenic clays. Continental weathering-derived clastics possess REY patterns identical to those of historically REY-rich phosphorites, characterized by light REY-rich signatures compared to heavy REY, typically contain higher REY content reaching several hundreds of ppm (Chen et al., 2013; Fu et al., 2019). In contrast, owing to the REY released into porewater during the alteration of terrigenous clastics are predominantly cap-

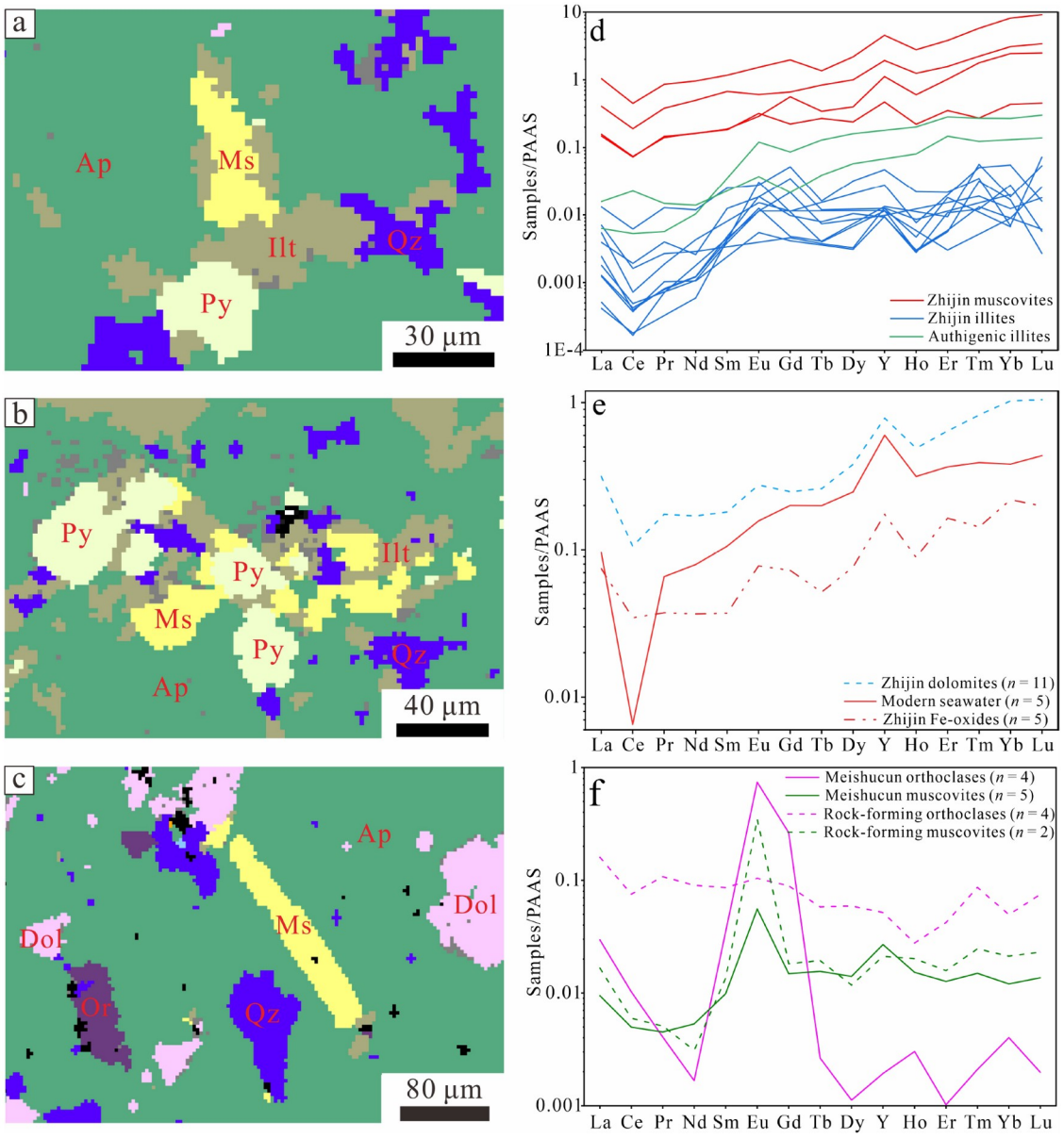

Figure 2 Mineral distributions and REY patterns in Zhijin and Meishucun phosphorites. (a) Illite formed around muscovite edges in Zhijin phosphorites. (b) Pyrite developed on residual muscovite substrates in Zhijin phosphorites. (c) Orthoclase and muscovite were randomly distributed in Meishucun phosphorites. (d) Zhijin clays and other authigenic illites exhibit heavy REY-rich distribution patterns, wherein the REY data of other authigenic illites cited from Uysal and Golding (2003). (e) Both the Zhijin dolomites and Fe-oxides exhibit heavy REY distribution patterns consistent with modern seawater. (f) Both the Meishucun orthoclases and muscovites exhibit flat REY distribution patterns consistent with rock-forming minerals. Abbreviation, Ap, Apatite; Qz, Quartz; Py, Pyrite; Ms, Muscovite; Ilt, illite; Or, Orthoclase; Dol, Dolomite.

tured by apatite, marine authigenic clay generally exhibits lower REY concentration with a heavy REY enriched pattern (Uysal and Golding, 2003) (Figure 2d). Thirdly, marine silicate alteration can modify both the elemental geochemical signatures and Si isotopic compositions of sediments. This alteration process not only tends to increase the Al concentration in sediments but also fractionantes the Si isotopic composition in silicate minerals, resulting in preferential enrichment of light Si isotopes (Geilert et al., 2023). For example, the δ^{30}Si values of terrestrial feldspars and kaolinites range from −0.63‰ to −0.29‰ and from −2.5‰ to −1.9‰, respectively, while marine silicate alteration-derived clay can exhibit δ^{30}Si value as low as −3.17‰ (Ziegler et al., 2005; Geilert et al., 2024). Thus, sediments affected by marine silicate alteration are expected to show lower δ^{30}Si values than unaltered ones (Figure S4a). Moreover, marine silicate alteration can produce a negative correlation between Al/Si ratios and Si isotopic compositions (Geilert et al., 2023). These mineralogical and geochemical differences serve as important criteria for distinguishing authigenic clay from clastic clay.

As described above, the mineralogical and geochemical

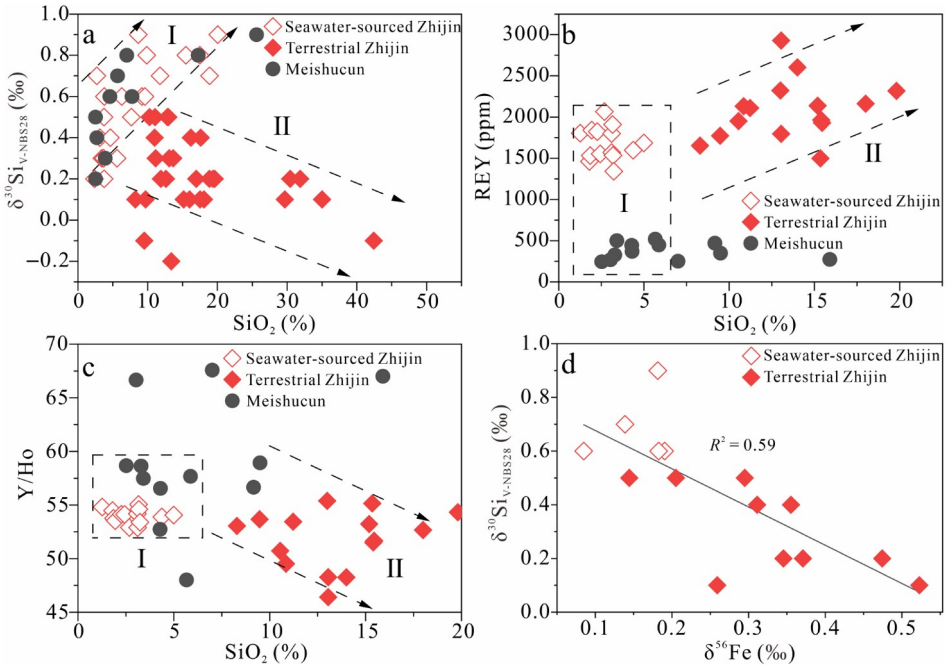

Figure 3 Relationships between Si-Fe isotopic compositions and phosphate REY enrichment. (a) Two sets of δ^{30}Si values from Zhijin and Meishucun phosphorites. One represents seawater endmember with higher δ^{30}Si values (average 0.6‰) and lower SiO_2 contents (average 8.10%). Another represents detrital endmember with a negative correlation between SiO_2 contents (average 17.45%) and δ^{30}Si values (average 0.2‰). (b, c) Two groups of REY data from Zhijin and Meishucun apatites. A set of REY indicates the influence of the seawater endmember with higher Y/Ho ratios (average 56) and lower REY contents (average 1076 ppm). Another set of REY reflects the detrital endmember influence with lower Y/Ho ratios (average 52) and higher REY contents (average 2085 ppm). (d) The δ^{56}Fe values of Zhijin phosphorites exhibit a negative correlation with their δ^{30}Si values, indicating a fluctuating oxic-suboxic marine environment promoted the decompostion of silicate minerals.

evidences support a distinction between the clay minerals in the Zhijin and Meishucun phosphorites. Firstly, muscovite in the Zhijin phosphorites shows irregular metasomatism by illite, with host-structured muscovite enclosing pyrite (Figure 2a, 2b). In contrast, Meishucun orthoclase and muscovite were randomly distributed, showing no evidence of such alteration (Figure 2c). Secondly, REY concentrations in Zhijin muscovite and illite range from 37.9 to 310 ppm and 0.44 to 3.49 ppm, respectively, with REY patterns similar to modern oxic seawater, authigenic illites, Zhijin dolomites, and Fe-oxides, but clearly distinct from those of Zhijin apatites and suspended sediment in World Rivers (SSWR, fine-grained clay) (Figure 2d, 2e, and Figure S6a). Notably, REY content of Zhijin illite (0.44–3.49 ppm) is much lower than that of SSWR and Zhijin apatites (~200 ppm and ~1500–2000 ppm) (Appendix Tables). This may be closely linked to the decomposition of Zhijin muscovite, which released REY into porewater that was subsequently captured by Zhijin apatite, suggesting an authigenic marine origin for Zhijin illite. However, Meishucun orthoclase and muscovite show REY patterns typical of continental rock-forming minerals, supporting their clastic origin (Figure 2f). These findings suggest significant REY exchange with seawater in Zhijin muscovite and illite, but not in Meishucun orthoclase and muscovite (REY, 2.69–6.45 ppm and 0.09–5.86 ppm, respectively). Thirdly, Zhijin samples generally exhibit higher Al contents (0.10%–6.53%) than Meishucun samples (0.05%–2.06%) (Appendix Tables). They also display lower δ^{30}Si values (−0.2‰ to 0.9‰, average 0.4‰) compared to Meishucun samples (0.2‰ to 0.9‰, average 0.6‰). Furthermore, both the Al/Si ratios and Si isotopic compositions of the Zhijin samples trend toward the authigenic clay endmember (Figure S4a). Besides, we noticed that two anomalous Meishucun phosphorites show high Al contents (1.57% and 2.06%), they exhibit elevated REY concentrations (303 ppm and 319 ppm) relative to the median REY concentrations in other Meishucun phosphorites (215 ppm) (Appendix Tables). This phenomenon may suggest intermediate processes between the Zhijin samples and other Meishucun samples, as supported by the sporadically observed minor illite growth along muscovite edges in Meishucun samples (Figures S3a, S3b).

In summary, the spatial distribution of minerals, REY concentrations and patterns in clay minerals, Al contents, Al/Si ratios, and δ^{30}Si data all evidenced that the Zhijin illites were formed through the marine silicate alteration of muscovites during early diagenesis.

5.2 How do clay minerals govern REY cycle

The δ^{30}Si values of authigenic clay formed through marine silicate alteration (−3.17‰ to −0.16‰) differ significantly

from those of dissolved oceanic silica (0.6‰–3.1‰) (Basile-Doelsch, 2006; Geilert et al., 2023, 2024). Using these as endmembers representing detrital mineral decomposition and seawater, respectively, Zhijin samples fall within an intermediate range of the δ^{30}Si values, indicating a mixture of seawater and detrital sources. In contrast, the Meishucun samples show higher δ^{30}Si values, suggesting a predominant seawater source (Figure S4a). By combining phosphate with higher Y/Ho ratios in seawater (~60) versus terrestrial sources (~28) (Abedini and Calagari, 2017), we identified two distinct groups in the dataset (Figure 3a–3c). The first group shows higher δ^{30}Si values (average 0.6‰) and Y/Ho ratios (average ~56), and lower SiO_2 (average 8.10%) and REY contents (average 1076 ppm), indicating a dominant seawater source for both Si and REY. The second group exhibits a negative correlation between δ^{30}Si values and SiO_2 contents, along with lower Y/Ho ratios (average ~52), and higher SiO_2 (average 17.45%) and REY contents (average 2085 ppm), suggesting a significant terrestrial contribution of both Si and REY in the Zhijin samples. Therefore, the δ^{30}Si data strongly suggested that marine silicate alteration transformed muscovite into illite, releasing REY into the porewater.

The supply of Si and Al is critical for the formation of authigenic clay minerals. Simulation experiments have shown that Fe-oxides can enhance the dissolution of siliceous materials through two primary mechanisms. First, Fe-oxides can adsorb dissolved Si from the ambient water, creating a larger concentration gradient between the surrounding water and Si saturation, promoting the continued dissolution of siliceous substances (Mayer et al., 1991). Second, experimental data indicated a Fe^{2+}/Si surface layer forms on silicate minerals. During oxidation, this layer was disrupted, causing Fe-oxide precipitation and the release of dissolved Si (as H_4SiO_4) into the porewater ($Fe^{2+}\rightarrow Fe^{3+}+e^-$, $Fe^{3+}+3H_2O\rightarrow Fe(OH)_3+3H^+$) (Morris and Fletcher, 1987). While experimental geochemical data supports the role of Fe-oxides in silicate mineral decomposition, natural fluctuations in redox environment may also facilitate this process. For instance, mineralogical studies have demonstrated the importance of Fe-oxides in the formation of authigenic nontronite in the Bauer Deep (Cole and Shaw, 1983). The oxic-suboxic phosphate nodules from the early Cambrian Niutitang Formation in South China show a strong positive correlation between REY concentrations (577–1470 ppm) and Al_2O_3 contents (0.32%–1.43%), and they recorded the conversion of potassium feldspar to hyalophane-quartz association (Gao et al., 2018). The aluminum likely originated from unstable Al-bearing minerals, such as muscovite, potentially sourced from the continent (Michalopoulos and Aller, 1995). These observations emphasize that fluctuating oxic-suboxic conditions not only facilitated Fe-oxide precipitation and dissolution but also initiated marine silicate alteration. Experimental evidence further supported a mechanistic link between the clay mineral dissolution, Fe redox cycle, and REY enrichment. For example, FeOOH-coated quartz substrates placed in anoxic Amazon shelf sediments (pH 7.2–7.4) rapidly precipitated K-Fe-Mg-enriched clay minerals, highlighting the role of redox driven clay formation in trace element cycling (Michalopoulos and Aller, 1995). Similarly, repeated weakly reducing conditions during continuous leaching of North Atlantic sediments have been shown to promote the migration of Al and Fe from silicate materials (Blaser et al., 2016). In the Zhijin phosphorites, Fe isotopic compositions exhibit a clear positive correlation with REY contents as well as a negative correlation with Si isotopic compositions (Figure 3d, Figure S5a). These patterns indicate that the Zhijin phosphorites not only formed in fluctuating oxic-suboxic marine environments (Zhang et al., 2022), but also such marine condition promoted the transformation of REY-rich muscovite into illite. This alteration released REY into the porewater, where they were subsequently captured by apatite. In contrast, the Meishucun phosphorites formed in fully oxidizing conditions (δ^{56}Fe≈0‰) (Zhang et al., 2022) (Figure S5a), and did not experience the geochemical processes and mineralogical transformations observed in the Zhijin phosphorites.

Previous studies on REY sources in the Zhijin phosphorites have identified contributions from both seawater and detrital sources, but have not quantified their respective proportions (Wu et al., 2022). Obviously, the PAAS-normalized REY pattern of Zhijin apatites closely resembles that of SSWR with heavy REY depletion (Figure S6a). This pattern is distinctly different from that of the Zhijin Fe-oxides with heavy REY enrichment (Figure 2e). Additionally, results from close-system experiment show a preferential release of light REY during the dissolution of detrital materials into porewater (Figure S6b). In this study, a negative correlation between the Y/Ho and Er_N/Lu_N ratios in Zhijin apatites (Figure S5b), also further indicates that REY enrichment in Zhijin apatites was co-controlled by seawater and terrigenous sources endmembers. However, the absence of these REY geochemical signatures and the elevated Y/Ho ratios in the Meishucun apatites suggest that their REY were predominantly sourced from seawater (Figure S5b). Therefore, to quantitatively assess the dual contribution of marine and terrestrial sources, we determined two-endmember mixing model using the REY composition of Zhijin's Fe-oxides (representing the marine endmember) and SSWR (serving as the terrestrial proxy). The model demonstrated that a critical threshold at 85% terrigenous-derived REY and 15% seawater-sourced REY, beyond which the characteristic heavy REY depletion pattern emerges in composite signatures (Figure S6c). This geochemical transition suggests that the marine-terrestrial REY cycling system—particularly the submarine dissolution of REY-rich detritus—dominated

the REY enrichment processes in phosphorites at the seawater/sediment interface. Terrigenous inputs are estimated to account for more than 80% of the REY inventory in the porewater, highlighting their major contribution to phosphorite REY enrichment.

5.3 Implication

REY enrichment mechanism in phosphorites, as identified in this study, can be summarized in three main stages: (1) REY, along with terrestrial minerals, were transported into ocean; (2) REY were released from these terrestrial minerals into the porewater during Fe redox cycling; and (3) REY were finally captured by apatite (Figure 4). This mechanism easily explains the REY enrichment in Cambrian phosphorites from the Nanhua Basin. Shelf-facies phosphorites generally have REY contents of ~200–400 ppm, examples as observed in the Meishucun and Bailongtan phosphorites from Yunnan Province, and the Jinsha and Xishui phosphorites from Guizhou Province (Chen et al., 2013). These phosphorites were deposited under fully oxidized shallow marine conditions and show limited evidence of terrigenous material alternation, which easily account for their low REY contents. However, REY enrichment in the shelf-facies Zhijin phosphorites was supported by both fluctuating redox conditions and the abundant supply of REY-rich terrigenous clastic. This difference in terrigenous input is further supported by the distinct $^{87}Sr/^{86}Sr$(i) ratios between Zhijin (0.7074–0.7092, average 0.7086) and Meishucun phosphorites (0.7103–0.7123, average 0.7113) (Liu and Zhou, 2020; Wu et al., 2022). The seawater $^{87}Sr/^{86}Sr$ ratio was estimated to be ~0.7080 during the Early Cambrian (~540 Ma) (Derry et al., 1994). Assuming the highest $^{87}Sr/^{86}Sr$(i) value (0.7123) in the Meishucun phosphorites represents the terrigenous endmember, the estimated terrigenous Sr contributions are ~13% for Zhijin phosphorites and ~73% for Meishucun, respectively. The relatively lower contribution of terrigenous Sr in the REY-rich Zhijin phosphorites may be attributed to the following factors: (1) Compared with REY (e.g., Y, 5100 years), Sr exhibits a longer marine residence time (~3–5×10^6 years) (Nozaki et al., 1997; Halverson et al., 2007); (2) Although the Zhijin phosphorites exhibit a relatively low proportion of terrigenous Sr contribution, the Zhijin muscovites contain significantly higher REY concentrations compared to those in the Meishucun. This implied that the source region of the Zhijin phosphorite was REY-rich, while the source region of the Meishucun phosphorite lacked significant REY enrichment; (3) With the increase in weathering intensity of continental granites, the Sr isotopic compositions of weathering profiles show a decreasing trend (Ma and Liu, 2001), implying that REY-rich source region may exhibit lower Sr isotopic characteristics. Additionally, compared to suspended particulate matters in the middle-lower Yangtze River, the suspended particulate matters from the upper Yangtze River near the source area display lower Sr isotopic compositions (Yang et al., 2007). Consequently, terrigenous

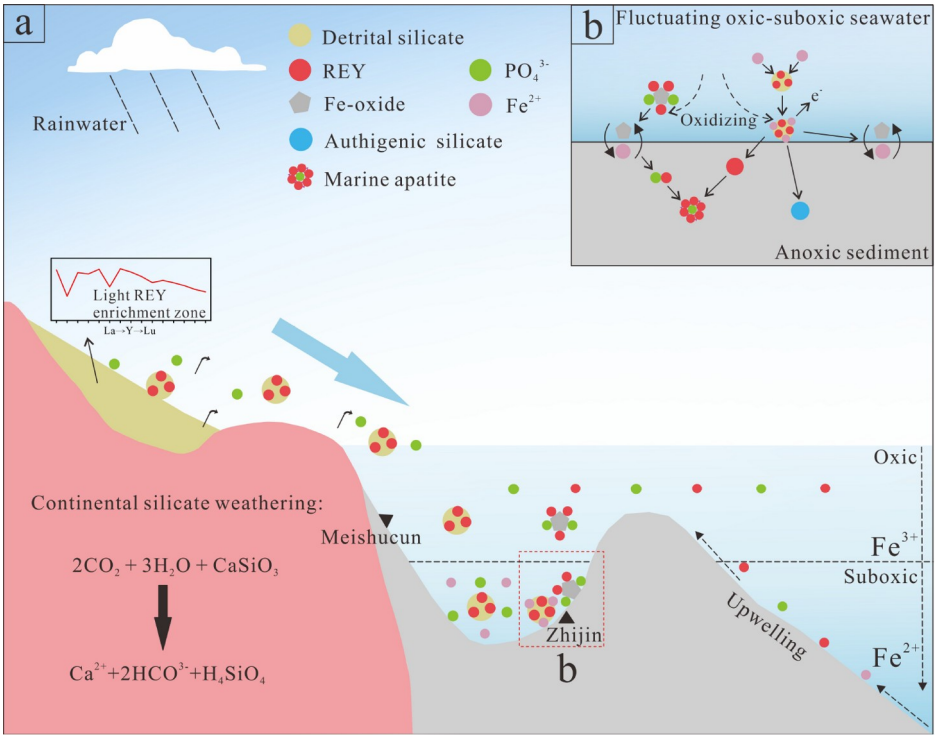

Figure 4 The model map between continental weathering and REY enrichment of marine phosphate.

clastic materials with lower Sr isotopic compositions releasing REY during decomposition might lead to a reduction in the Sr isotopic composition of local seawater. Additionally, phosphorus nodules from slope facies generally show much higher REY contents (~500–1500 ppm) (Chen et al., 2013; Gao et al., 2018). These slope facies were dominated by suboxic or ferruginous seawater conditions during the early Cambrian (Wen et al., 2015). The REY contents of these nodules exhibit a negative correlation with Y/Ho ratios (31–54), indicating a significant terrestrial REY contribution. In these settings, as in the Zhijin phosphorites, the decomposition of terrestrial minerals was driven by fluctuating redox conditions, releasing REY into the porewater.

The new mechanism proposed in our study could be a universal process that helps explain the variability of REY contents in global phosphorites throughout geological history. For instance, Upper Cretaceous-Eocene phosphorites, which were deposited a under highly oxic sedimentary conditions and display seawater-like REY patterns, generally show low REY contents (averaging 27.4 ppm) (Sefik Imamoglu et al., 2009). It's noted that ancient phosphorites with REY patterns similar to Zhijin phosphorites, often show relatively low REY contents. For example, Paleoproterozoic and early Cambrian phosphorites from India and northern Iran contain REY contents in the ranges of 2.89–38.6 ppm and 96.3–226 ppm, respectively, although they experienced an active Fe redox cycle at the seawater-sediment interface (Khan et al., 2012b; Abedini and Calagari, 2017). These relatively low REY contents were ascribed to a limited supply of terrigenous sediments (Khan et al., 2012a, 2012b; Abedini and Calagari, 2017). Finally, the high total REY contents of up to 800 ppm and 1500 ppm in those Early and Middle Cambrian phosphorites from Montagne Noire (France) and Scania (Sweden), respectively, can be attributed to the input of felsic clastic materials from a magmatic source and associated marine silicate alternation (e.g., Quartz and K-feldspar deposited within apatite, pyrite developed on ferrous silicate substrates) (Álvaro et al., 2016). Similarly, the clastic rocks and phosphorite deposits from the late Ediacaran Kalyus Beds (East European Platform) were derived from felsic or mafic source rocks, indicating a predominantly terrestrial REY source (Francovschi et al., 2020). In the Georgina Basin, Australia, Cambrian phosphorite REY enrichment has been linked to interactions between surface and groundwater with granitic or schistose metasedimentary basement rocks (Valetich et al., 2022). Further examples include middle Permian and upper Devonian phosphate grains from Montana and Kentucky, USA, which exhibit extremely high REY contents up to ~2000 ppm and ~10000 ppm, respectively (Emsbo et al., 2015). Although the REY enrichment mechanism in USA phosphorites has not been fully investigated, Y/Ho ratios provide insight into source contributions. The Kentucky phosphates exhibit terrigenous-like Y/Ho ratios (34–39), whereas the Montana phosphates display marine-like ratios (~60), suggesting varying degrees of seawater versus terrestrial influence on REY enrichment.

Notably, modern deep-sea muds from the Pacific Ocean also contain high REY concentrations, ranging from 1000 to 2000 ppm, with the REY primarily hosted in apatite and exhibiting terrestrial-like Y/Ho ratios (22–28) (Kato et al., 2011). Furthermore, these apatites show negative Nd isotope signatures (ε_{Nd}, −6 to −10) and REY patterns similar to those of phillipsites (REY, 19.0–140 ppm) (Bi et al., 2021; Zhang et al., 2023). Additionally, in carbonate ooze sediments and porewater at the seafloor, a significant positive correlation between Al and REY contents further suggested that REY were primarily originated from aluminosilicate minerals (Bi et al., 2021; Deng et al., 2022). Therefore, despite the lack of direct evidence of Si isotopic compositions, previous studies based on mineralogical and elemental geochemical investigations have preliminarily proposed that REY enrichment in modern Pacific Ocean sediments was associated with the oxidation of seafloor hydrothermal Fe^{2+} and the early diagenetic silicate dissolution (Hu et al., 2024; Wang et al., 2024). In any case, the decomposition of detrital minerals and subsequent REY release warrant significant attention, as it provided a new perspective for understanding REY enrichment mechanisms in marine sedimentary environment.

6. Conclusions

Our study elucidates the critical role of clay minerals in the REY enrichment of marine phosphorites, particularly highlighting the significance of authigenic illite formed through marine silicate alteration. The contrasting REY patterns observed in Zhijin and Meishucun clays underscored the influence of fluctuating redox condition and terrigenous input on REY geochemistry. In the Zhijin phosphorites, significant REY enrichment is linked to the transformation of muscovite into illite, which facilitated REY release into porewater. In contrast, the Meishucun phosphorites exhibit limited REY enrichment, attributed to persistently oxidizing conditions and a lower supply of REY-rich terrigenous material. These findings challenge the traditional view that REY enrichment in phosphorites is primarily driven by the Fe redox pump. Instead, our results underscore the importance of marine silicate alteration of terrigenous REY-rich minerals at the seawater-sediment interface, offering a more nuanced understanding of REY enrichment mechanisms throughout geological history. This framework also provides a valuable basis exploring REY-rich marine sediments on a global scale.

Acknowledgements *We sincerely thank the academic editor and anonymous reviewers for their thorough evaluation and constructive sug-*

gestions during the peer-review process. This research was supported by the National Natural Science Foundation of China (Grant Nos. 92062221, 42121003), Jiangxi Province Key Laboratory of Exploration and Development of Critical Mineral Resources (Grant No. GJKC2024ZZ07), Guizhou Provincial Science and Technology Subsidies (Grant Nos. GZ2020SIG, GZ2021SIG), and Geological Exploration Fund of Guizhou Province (Grant No. 2024-2).

Conflict of interest The authors declare that they have no conflict of interest.

Supporting information The supporting information is available online at http://earth.scichina.com and http://link.springer.com. The supporting materials are published as submitted, without typesetting or editing. The responsibility for scientific accuracy and content remains entirely with the authors.

References

Abbott A N, Löhr S, Trethewy M. 2019. Are clay minerals the primary control on the oceanic rare earth element budget? Front Mar Sci, 6: 504

Abedini A, Calagari A A. 2017. REEs geochemical characteristics of lower Cambrian phosphatic rocks in the Gorgan-Rasht Zone, northern Iran: Implications for diagenetic effects and depositional conditions. J African Earth Sci, 135: 115–124

Adebayo S B, Cui M, Williams T J, Martin E, Johannesson K H. 2022. Evolution of rare earth element and ε_{Nd} compositions of Gulf of Mexico seawater during interaction with Mississippi River sediment. Geochim Cosmochim Acta, 335: 231–242

Álvaro J J, Shields-Zhou G A, Ahlberg P, Jensen S, Palacios T, Fairchild I. 2016. Ediacaran-Cambrian phosphorites from the western margins of Gondwana and Baltica. Sedimentology, 63: 350–377

Basile-Doelsch I. 2006. Si stable isotopes in the Earth's surface: A review. J Geochem Explor, 88: 252–256

Berner R A, Holdren G R. 1977. Mechanism of feldspar weathering: Some observational evidence. Geology, 5: 369–372

Bi D, Shi X, Huang M, Yu M, Zhou T, Zhang Y, Zhu A, Shi M, Fang X. 2021. Geochemical and mineralogical characteristics of deep-sea sediments from the Western North Pacific Ocean: Constraints on the enrichment processes of rare earth elements. Ore Geol Rev, 138: 104318

Blaser P, Lippold J, Gutjahr M, Frank N, Link J M, Frank M. 2016. Extracting foraminiferal seawater Nd isotope signatures from bulk deep sea sediment by chemical leaching. Chem Geol, 439: 189–204

Chen J, Yang R, Wei H, Gao J. 2013. Rare earth element geochemistry of Cambrian phosphorites from the Yangtze Region. J Rare Earths, 31: 101–112

Cole T G, Shaw H F. 1983. The nature and origin of authigenic smectites in some recent marine sediments. Clay miner, 18: 239–252

Compston W, Zhang Z, Cooper J A, Ma G G, Jenkins R J F. 2008. Further SHRIMP geochronology on the early Cambrian of South China. Am J Sci, 308: 399–420

Deng Y, Guo Q, Zhu J, He G, Yang Y, Cao J, Ren J, Liu Y, Famiyeh L, Guo B, Wang H, Liao J, Zhou J, Cheng S, Zhao B, Jiang X. 2022. Significant contribution of seamounts to the oceanic rare earth elements budget. Gondwana Res, 112: 71–81

Derry L A, Brasier M D, Corfield R M, Rozanov A Y, Zhuravlev A Y. 1994. Sr and C isotopes in lower Cambrian carbonates from the Siberian craton: A paleoenvironmental record during the 'Cambrian explosion'. Earth Planet Sci Lett, 128: 671–681

Ding T. 2004. Analytical Methods for Silicon Isotope Determinations. In: de Groot P A, ed. Handbook of Stable Isotope Analytical Techniques. Amsterdam: Elsevier. 523–537

Emsbo P, McLaughlin P I, Breit G N, du Bray E A, Koenig A E. 2015. Rare earth elements in sedimentary phosphate deposits: Solution to the global REE crisis? Gondwana Res, 27: 776–785

Francovschi I, Grădinaru E, Roban R D, Ducea M N, Ciobotaru V, Shumlyanskyy L. 2020. Rare earth element (REE) enrichment of the late Ediacaran Kalyus Beds (East European Platform) through diagenetic uptake. Geochemistry, 80: 125612

Fu W, Li X, Feng Y, Feng M, Peng Z, Yu H, Lin H. 2019. Chemical weathering of S-type granite and formation of Rare Earth Element (REE)-rich regolith in South China: Critical control of lithology. Chem Geol, 520: 33–51

Gao P, He Z, Li S, Lash G G, Li B, Huang B, Yan D. 2018. Volcanic and hydrothermal activities recorded in phosphate nodules from the lower Cambrian Niutitang Formation black shales in South China. Palaeogeogr Palaeoclimatol Palaeoecol, 505: 381–397

Geilert S, Frick D A, Abbott A N, Löhr S C. 2024. Marine clay maturation induces systematic silicon isotope decrease in authigenic clays and pore fluids. Commun Earth Environ, 5: 573

Geilert S, Frick D A, Garbe-Schönberg D, Scholz F, Sommer S, Grasse P, Vogt C, Dale A W. 2023. Coastal El Niño triggers rapid marine silicate alteration on the seafloor. Nat Commun, 14: 1676

Haley B A, Klinkhammer G P, McManus J. 2004. Rare earth elements in pore waters of marine sediments. Geochim Cosmochim Acta, 68: 1265–1279

Halverson G P, Dudás F Ö, Maloof A C, Bowring S A. 2007. Evolution of the $^{87}Sr/^{86}Sr$ composition of Neoproterozoic seawater. Palaeogeogr Palaeoclimatol Palaeoecol, 256: 103–129

Hu Q, Shi X, Bi D, Yu M, Huang M, Li J, Liu J, Zhou T, Song Z, Li C, Zhu A, Zhang H. 2024. Transfer of rare earth elements from clay-sized fraction to phosphate in East South Pacific Ocean: Implication for REY-rich sediment related to hydrothermal influence. Ore Geol Rev, 174: 106294

Jeandel C, Oelkers E H. 2015. The influence of terrigenous particulate material dissolution on ocean chemistry and global element cycles. Chem Geol, 395: 50–66

Kato Y, Fujinaga K, Nakamura K, Takaya Y, Kitamura K, Ohta J, Toda R, Nakashima T, Iwamori H. 2011. Deep-sea mud in the Pacific Ocean as a potential resource for rare-earth elements. Nat Geosci, 4: 535–539

Khan K F, Dar S A, Khan S A. 2012a. Geochemistry of phosphate bearing sedimentary rocks in parts of Sonrai block, Lalitpur District, Uttar Pradesh, India. Geochemistry, 72: 117–125

Khan K F, Dar S A, Khan S A. 2012b. Rare earth element (REE) geochemistry of phosphorites of the Sonrai area of Paleoproterozoic Bijawar basin, Uttar Pradesh, India. J Rare Earths, 30: 507–514

Liu Y S, Hu Z C, Gao S, Günther D, Xu J, Gao C G, Chen H H. 2008. *In situ* analysis of major and trace elements of anhydrous minerals by LA-ICP-MS without applying an internal standard. Chem Geol, 257: 34–43

Liu Z R R, Zhou M F. 2017. , Meishucun phosphorite succession (SW China) records redox changes of the early Cambrian ocean. GSA Bull, 129: 1554–1567

Liu Z R R, Zhou M F. 2020. Early Cambrian ocean mixing recorded by phosphorite successions in the Nanhua Basin, South China. Precambrian Res, 349: 105414

Ma Y, Liu C. 2001. Sr isotope evolution during chemical weathering of granites. Sci China Ser D-Earth Sci, 44: 726–734

Mayer L M, Jorgensen J, Schnitker D. 1991. Enhancement of diatom frustule dissolution by iron oxides. Mar Geol, 99: 263–266

Menendez A, James R H, Roberts S, Peel K, Connelly D. 2017. Controls on the distribution of rare earth elements in deep-sea sediments in the North Atlantic Ocean. Ore Geol Rev, 87: 100–113

Michalopoulos P, Aller R C. 1995. Rapid clay mineral formation in Amazon delta sediments: Reverse weathering and oceanic elemental cycles. Science, 270: 614–617

Morris R C, Fletcher A B. 1987. Increased solubility of quartz following ferrous-ferric iron reactions. Nature, 330: 558–561

Nozaki Y, Zhang J, Amakawa H. 1997. The fractionation between Y and Ho in the marine environment. Earth Planet Sci Lett, 148: 329–340

Paul S A L, Volz J B, Bau M, Köster M, Kasten S, Koschinsky A. 2019.

Calcium phosphate control of REY patterns of siliceous-ooze-rich deep-sea sediments from the central equatorial Pacific. Geochim Cosmochim Acta, 251: 56–72

Ren J B, Jiang X X, He G W, Wang F L, Yang T B, Luo S J, Deng Y A, Zhou J H, Deng X G, Yao H Q, Yu H X. 2022. Enrichment and sources of REY in phosphate fractions: Constraints from the leaching of REY-rich deep-sea sediments. Geochim Cosmochim Acta, 335: 155–168

Sefik Imamoglu M, Nathan Y, Çoban H, Soudry D, Glenn C. 2009. Geochemical, mineralogical and isotopic signatures of the Semikan, West Kasrık "Turkish" phosphorites from the Derik-Mazıdağı-Mardin area, SE Anatolia. Int J Earth Sci-Geol Rund, 98: 1679–1690

Uysal I T, Golding S D. 2003. Rare earth element fractionation in authigenic illite-smectite from Late Permian clastic rocks, Bowen Basin, Australia: Implications for physico-chemical environments of fluids during illitization. Chem Geol, 193: 167–179

Valetich M, Zivak D, Spandler C, Degeling H, Grigorescu M. 2022. REE enrichment of phosphorites: An example of the Cambrian Georgina Basin of Australia. Chem Geol, 588: 120654

Wang Y J, Shi X, Huang M, Yu M, Hu N, Ren X, Liu J, Zhu A, Bi D, Zhang Y. 2024. Importance of early diagenesis of deep-sea sediments to the REY enrichment and oceanic element budget. Ore Geol Rev, 167: 105980

Wen H, Fan H, Zhang Y, Cloquet C, Carignan J. 2015. Reconstruction of early Cambrian ocean chemistry from Mo isotopes. Geochim Cosmochim Acta, 164: 1–16

Wu S W, Fan H F, Xia Y, Meng Q T, Gong X X, He S, Liu X Q, Yang H Y, Wen H J. 2022. Sources of rare earth elements and yttrium in the early Cambrian phosphorites in Zhijin, southwest China. Ore Geol Rev, 150: 105146

Xing J, Li S, Wei H, Xi J, Lin X, Yang Y, Xian H, Tan W, Wei J, Zhu J. 2024. Influence of goethite nanophase on rare-earth element patterns and enrichment in marine phosphates during early diagenesis. Chem Geol, 653: 122029

Xu L G, Lehmann B, Mao J W, Qu W J, Du A D. 2011. Re-Os age of polymetallic Ni-Mo-PGE-Au mineralization in early Cambrian black shales of South China—A reassessment. Econ Geol, 106: 511–522

Yang S Y, Jiang S Y, Ling H F, Xia X P, Sun M, Wang D J. 2007. Sr-Nd isotopic compositions of the Changjiang sediments: Implications for tracing sediment sources. Sci China Ser-D Earth Sci, 50: 1556–1565

Yuan G, Cao Y, Schulz H M, Hao F, Gluyas J, Liu K, Yang T, Wang Y, Xi K, Li F. 2019. A review of feldspar alteration and its geological significance in sedimentary basins: From shallow aquifers to deep hydrocarbon reservoirs. Earth-Sci Rev, 191: 114–140

Zhang H, Fan H, Wen H, Han T, Zhou T, Xia Y. 2022. Controls of REY enrichment in the early Cambrian phosphorites. Geochim Cosmochim Acta, 324: 117–139

Zhang X, Lu Y, Miao Y, Huang M, Zhu K, Cai L, Wang J, Shi X. 2023. Radiogenic Nd in bioapatite from rare earth elements rich deep sea sediments from Central Indian Oceanic Basin and its implication in material sources. Ore Geol Rev, 154: 105295

Zhao L, Chen Z Q, Algeo T J, Chen J, Chen Y, Tong J, Gao S, Zhou L, Hu Z, Liu Y. 2013. Rare-earth element patterns in conodont albid crowns: Evidence for massive inputs of volcanic ash during the latest Permian biocrisis? Glob Planet Change, 105: 135–151

Zhu R X, Li X H, Hou X G, Pan Y X, Wang F, Deng C L, He H Y. 2009. SIMS U-Pb zircon age of a tuff layer in the Meishucun section, Yunnan, southwest China: Constraint on the age of the Precambrian-Cambrian boundary. Sci China Ser D-Earth Sci, 52: 1385–1392

Ziegler K, Chadwick O A, White A F, Brzezinski M A. 2005. δ^{30}Si systematics in a granitic saprolite, Puerto Rico. Geology, 33: 817–820

(Editorial handling: Huayong CHEN)